ACS APPLIED MATERIALS & INTERFACES

Research Article

www.acsami.org

In situ Assembly of Raspberry- and Mulberry-like Silica Nanospheres toward Antireflective and Antifogging Coatings

Xiaoyu Li[†,‡] and Junhui He*[,†]

[†]Functional Nanomaterials Laboratory and Key Laboratory of Photochemical Conversion and Optoelectronic Materials, Technical Institute of Physics and Chemistry, Chinese Academy of Sciences (CAS), Zhongguancundonglu 29, Haidianqu, Beijing 100190, China

[‡]Graduate University of Chinese Academy of Sciences, Beijing 100864, China

Supporting Information

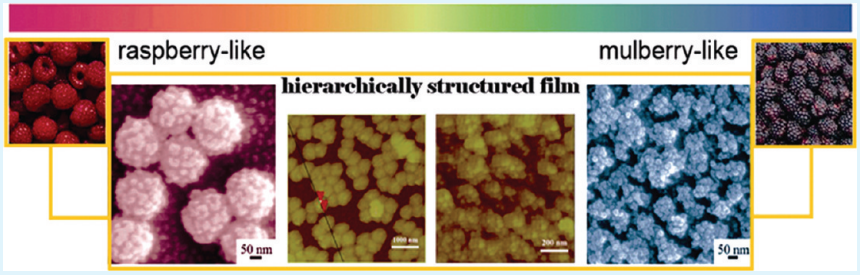

ABSTRACT: Raspberry- and mulberry-like hierarchically structured silica particulate coatings were fabricated via facile in situ layer-by-layer assembly with monodisperse silica nanoparticles (NPs) of two different sizes followed by calcination. Raspberry-like and mulberry-like silica particulate coatings were achieved when the size ratio of two silica particles was 20/200 and 20/70 nm, respectively. The latter coating exhibited good antireflective property. Its maximum transmittance reached as high as 97%, whereas that of the glass substrate is only 91%. The morphologies of the coatings were observed by scanning electron microscopy and atom force microscopy. The surface properties of these coatings were investigated by measuring their water contact angles and the spreading time of water droplet. The results showed that such hierarchically structured coatings had superhydrophilic and antifogging properties.

KEYWORDS: *superhydrophilic, antifogging, raspberry-like silica nanoparticle, mulberry-like silica nanoparticle, LbL assembly*

1. INTRODUCTION

Hierarchically structured porous films have been attracting much attention in applications ranging from chemical sensors,[1] antireflective films,[2] catalysts,[3−5] and biomaterials engineering[6−8] to superhydrophilic[9−21] and superhydrophobic films.[22−31] Various approaches have been developed to construct hierarchically structured porous films including hard or soft template method, electrochemical deposition, phase separation of polymer, domain-selective treatment by etching or lithography, hydrothermal reaction and self-assembly.[32−40]

Electrostatic layer-by-layer (LbL) assembly is of special interest because it is a green, simple, and easily controllable method to assemble porous films on varied substrates, such as glass, silicon wafer, and other flexible substrates. This bottom-up approach allows easy design and control over the film structure and thus improving their performances. Thus, more and more works focus on preparing hierarchically structured films with multifunctional properties by LbL assembly. The LbL assembly has been used for constructing films with hierarchically rough surfaces in two different ways. One employs NPs with dual-size roughness, such as raspberry-like nanoparticles (NPs).[41−43] For example, we reported films of raspberry-like silica nanospheres and silica hollow nanospheres that show excellent superhydrophilic and antifogging properties.[28,30,31] However, such building blocks must be prepared before the assembly of films, which is, in most cases if not all, relatively complex. For example, the fabrication procedure of raspberry-like silica nanospheres includes alternate modification of PDDA and PSS and subsequent assembly of smaller silica NPs on the surface of core silica nanospheres (Scheme 1a). After each assembly, redundant polyelectrolytes must be removed by rinsing and centrifugation.[30] Raspberry-like silica hollow nanospheres were also fabricated using polystyrene (PS) nanospheres as core in a similar way.[28] In another attempt, oxygen plasma treatment was used toward the surface of PS spheres to produce hydroxyl groups, and raspberry-like silica hollow nanospheres were achieved in one-step sol−gel method followed by calcination.[31] In this approach, careful modification of the PS sphere surface and regulation of the amount of tetraethyl orthosilicate (TEOS) are necessary and relatively complex. Similar raspberry particles can be also prepared by heterocoagulation of oppositely charged particles of two

Received: February 7, 2012
Accepted: March 26, 2012
Published: March 26, 2012

Scheme 1. Schematic Illustration of Particulate Films Assembled from (a) Pre-and (b) In situ Fabricated Raspberry-like Particles

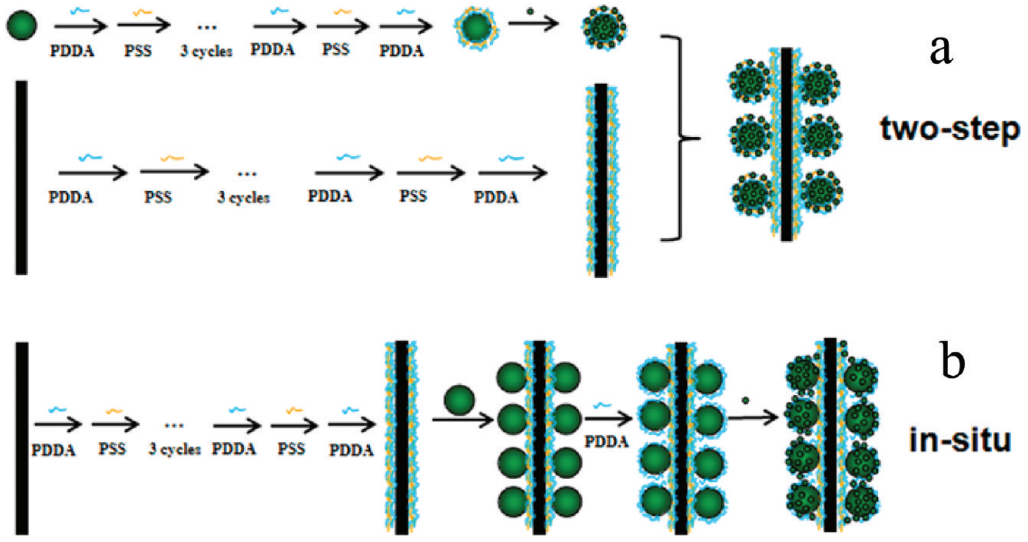

specific diameters.[41,42] What's more, the self-assembly of raspberry-like particles becomes less efficient on oppositely charged substrates, because they are relatively hard to roll on the flat substrate surface due to their intrinsic rough shapes. The rolling character is believed to be necessary for efficient self-assembly. Clearly, the two-step methods are relatively complex and time-consuming. The other way to prepare hierarchically structured films uses nanoparticles of varied sizes, and constructs hierarchically rough surfaces via their rational combination.[29,44] Thus, raspberry-like particulate films may be fabricated by in situ assembly of multisize and/or multimaterial building blocks (Scheme 1b).

In the current work, a simple, in situ method was developed to fabricate hierarchically structured silica nanoparticles surfaces by LbL assembly. Unlike the assembly of special dual-size roughness NPs, common solid nanospheres with varied sizes were used to construct hierarchically rough surfaces via their rational combination. Larger particles were effectively adsorbed on substrate, followed by adsorption of smaller silica NPs on the surface of larger particles, directly giving hierarchically structured porous films of raspberry-like particles. Exciting superhydrophilic and antifogging properties were achieved on these films. By controlling the size ratio of dual-size particles, mulberry-like nanoparticles film with both good antireflective and antifogging properties were also fabricated. For a high transmittance of 97%, the number of adsorption cycles was cut down to only 5 cycles, as compared with 12 cycles needed in our previous work.[29] These results would give some indication for fabrication of hierarchically structured films by balancing the porosity and surface roughness via interesting assembly design.

2. EXPERIMENTAL SECTION

Materials. Tetraethyl orthosilicate (TEOS, 99+%), sodium poly(4-styrenesulfonate) (PSS, M_w = 70 000) were obtained from Alfa Aesar. Poly(diallyldimethylammonium chloride) (PDDA, M_w = 200 000–350 000, 20 wt %) was purchased from Aldrich. Aqueous ammonia (25%), concentrated sulfuric acid (98%), hydrogen peroxide (30%), and absolute ethanol (99.5%) were purchased from Beihua Fine Chemicals. Ultrapure water with a resistivity higher than 18.2 MΩ·cm was used in all experiments, and was obtained from a three-stage Millipore Mill-Q Plus 185 purification system (Academic). Monodisperse SiO_2 NPs of ca. 20 nm (S-20), ca. 70 nm (S-70), ca. 100 nm (S-100), ca.150 nm (S-150), and ca.200 nm (S-200) were prepared according to the Stöber method,[46] from which were prepared SiO_2 suspensions of 0.1 wt % with absolute ethanol. The as-prepared suspensions of 20 and 70 nm SiO_2 nanoparticles had a pH value of nearly 10, and were used directly. The 100, 150 and 200 nm SiO_2 NPs were centrifuged, washed with pure water, and redispersed in absolute ethanol. The pH values of these obtained suspensions were adjusted to 10 by using aqueous ammonia (25%).

Thin Film Assembly. The procedure for preparation of superhydrophilic and antireflective coatings is described as follows. First, glass or silicon substrates were cleaned with Piranha solution (98 wt % H_2SO_4/30 wt % H_2O_2, 7/3 v/v), and then washed with water (Caution: the Pirhana solution is highly dangerous and must be used with great care). The cleaned substrates were alternately dipped in PDDA and PSS solutions for 5 min, and redundant polyelectrolytes were removed by shaking in pure water for 2 min and rinsing for 1 min followed by drying with N_2 flow. The concentrations of PDDA and PSS aqueous solutions were 2 mg mL^{-1}. Multilayers of $(PDDA/PSS)_5$/PDDA were prepared, and were used as a primer in all experiments. Second, the $(PDDA/PSS)_5$/PDDA covered substrates were alternately dipped in prepared SiO_2 suspensions of varied SiO_2 particle sizes (0.1 wt %) and an PDDA solution (2 mg mL^{-1}) by the same procedure for an appropriate number of cycles. Finally, the as-prepared coatings were blown dry with N_2 flow at room temperature and calcinated (heating rate: 5 °C min^{-1}) at 550 °C for 3 h to remove the polyelectrolytes.

Characterization. For transmission electron microscopy (TEM) observations, powder samples were added on carbon-coated copper grids, and observed on a JEOL JEM-2100F transmission electron microscope at an acceleration voltage of 200 kV. Freshly fabricated coatings were examined by scanning electron microscopy (SEM) on a Hitachi S-4300 scanning electron microscope operated at 10 kV. Water contact angles (WCAs) of surfaces were measured at ambient temperature on a JC2000C contact angle/interface system (Shanghai Zhongchen Digital Technique Apparatus Co.). Water droplets of 3 μL were dropped carefully onto the sample surfaces. Transmittances in the range between 300 and 800 nm were recorded using a TU-1901 spectrophotometer (Beijing Purkinje General Instrument Co.) Atomic force microscopy (AFM) images were taken with a Nanoscope IIIa AFM Multimode system under ambient conditions. AFM was operated in the tapping mode by using silicon nitride cantilevers. An ellipsometer (Semilab, GES5E) was used to measure the refractive index (n) and thickness of prepared films.

3. RESULTS AND DISCUSSION

Thin Film Assembly and Characterization. The current in situ approach to the fabrication of hierarchically structured raspberry-like coatings is schematically illustrated in Scheme 1. Unlike the two-steps method, it can fabricate similar hierarchically structured raspberry-like coatings but without the complex prepreparation of hierarchically structured nanoparticles. Hierarchically structured raspberry-like particles coatings of varied morphologies could be assembled from simple silica NPs with dual sizes.

As showed in Figure 1a and b, a slide glass was modified on its surface with PDDA, which is positively charged and is able to adsorb negatively charged silica NPs (200 nm in diameter) through electrostatic interactions. After subsequent modification of the particulate film with PDDA treatment, small NPs (20 nm in diameter) were adsorbed on the particulate film to construct a secondary structure, leading to a surface with a raspberry-like morphology. In Figure 1b, it is seen that the 20 nm silica NPs were adsorbed on both glass substrate and the large silica nanospheres. The coating is similar in morpholgy to previously reoported coatings.[28,30,31] However, unlike the raspberry-like nanoparticle films fabricated by the two-step method, the dual-size nanoparticles prepared by the in situ approach are halves of raspberry-like nanoparticles, and the bottom halves are smooth and attached to the surface of substrate. Clearly, the in situ fabricated raspberry-like particle films maintain the similar rough surface as the two-step method. The rolling resistance of prefabricated raspberry-like particles is larger than that of smooth nanospheres so that the coverage degree of prefabricated raspberry-like particles is only ca. 50% or lower on the substrate.[31] However, the raspberry-like particulate films could be fabricated by the in situ method with high coverage degree of particles because of the easy assembly of spherical building blocks.

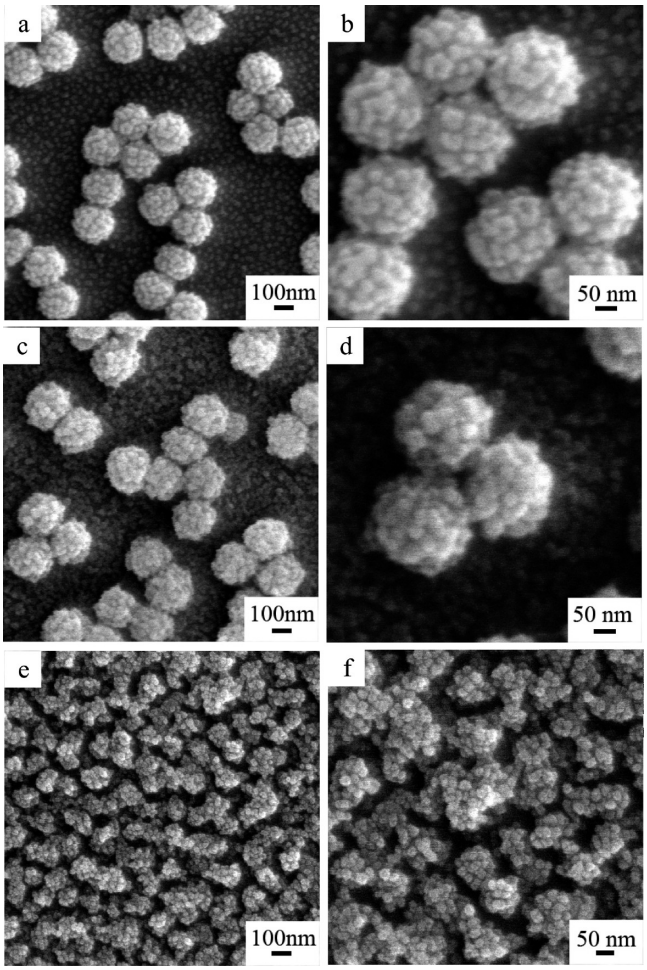

Figure 1. SEM images of LbL deposited (a) $(PDDA/S\text{-}200)_1(PDDA/S\text{-}20)_1$, (c) $(PDDA/S\text{-}200)_1(PDDA/S\text{-}20)_2$, and (e) $(PDDA/S\text{-}70)_1(PDDA/S\text{-}20)_4$ coatings. (b, d, f) Magnified views of a, c, and e, respectively.

The area number density of silica NPs of coatings prepared by the in situ method could be tuned by changing the size of particles or the number of deposition cycles. Figure 1c and d show SEM images of the particulate film after applying one more deposition cycle of 20 nm silica nanopartilces on the 200 nm particulate film. Apparently, the surface coverage of small particles increased due to the increase of deposition cycles. More compact raspberry-like silica NPs films were obtained, as compared with that of one deposition cycle of 20 nm silica nanopartilces in Figure 1a,b. Clearly, more 20 nm silica NPs are adsorbed on the uncovered surface or on top of 200 nm NPs, which is believed to be advantageous for forming a rougher surface. We used AFM to further characterize the particulate films. Figure 2 shows the AFM topography image and height profile of $(PDDA/S\text{-}200)_1(PDDA/S\text{-}20)_2$. The topography observed by AFM agrees well with that observed by SEM (Figures 1a and 2a). The coverage of ca. 200 nm particles on the substrate is over 50%, and the surfaces of both large particles and substrate are covered with small nanoparticles. The vertical distance between two arrows is 234.8 nm which approximates the sum of diameters of two particles (200 and 20 nm). Although extremely small pores were not accessible by AFM tip, AFM was still an important and effective tool to estimate the surface roughness of coatings. Table 1 shows that the root-mean-square (rms) roughnesses of $(PDDA/S\text{-}200)_1(PDDA/S\text{-}20)_2$, $(PDDA/S\text{-}200)_1(PDDA/S\text{-}20)_1$ and $(PDDA/S\text{-}200)_1$ are 99.5, 83.1, and 73.0 nm, respectively. The rms roughness of glass slide is only 2.6 nm. Thus, deposition of small nanoparticles on the substrate significantly increased the surface roughness. Therefore, the rms roughness of hierarchically structured films could increase by increasing deposition cycles of 20 nm nanoparticles. The surface roughness is believed to affect both the transmittance and wetting property of coatings, which is discussed below in detail

To better understand the relationship between the raspberry-like structure and the size ratio of large and small silica particles, we also prepared coatings using silica particles of different size ratios. We chose 70, 100, and 150 nm silica particles to substitute for 200 nm particles so that the size ratio was 20/70, 20/100, and 20/150, respectively. It was found that only when the size ratio was 20/200 (1/10), fine raspberry-like structures were constructed. Considering the need of construction of AR coatings (the optimal thickness is quarter-wavelength of incidence light), three bilayers of PDDA and 20 nm silica NPs ($(PDDA/S\text{-}20)_3$) were also used as a primer for enhancing transmittance. The surface morphologies of these films, i.e., $(PDDA/S\text{-}20)_3(PDDA/S\text{-}70)_1(PDDA/S\text{-}20)_1$, $(PDDA/S\text{-}20)_3(PDDA/S\text{-}100)_1(PDDA/S\text{-}20)_1$, and $(PDDA/S\text{-}20)_3(PDDA/S\text{-}150)_1(PDDA/S\text{-}20)_1$ are showed in Figure S1 in the Supporting Information. Clearly, dual-scale structured surfaces could also be constructed using these pairs of silica particles. However, few raspberry-like nanostructures formed

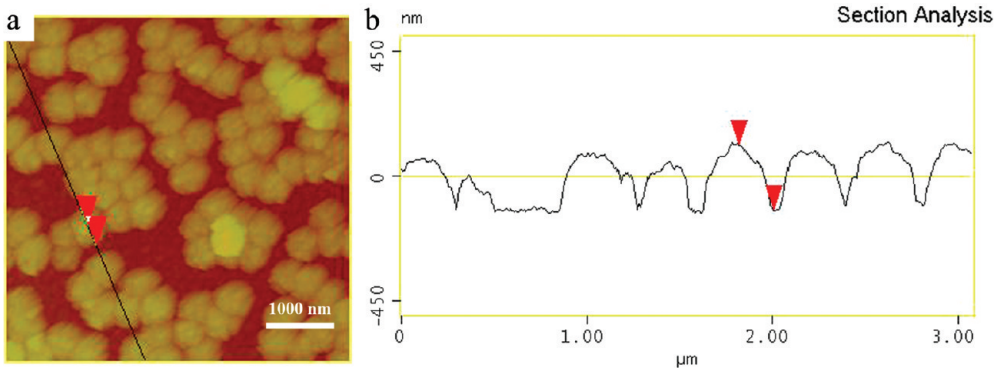

Figure 2. (a) AFM taping mode topography image and (b) height profile of the surface of $(PDDA/S\text{-}200)_1(PDDA/S\text{-}20)_1$.

Table 1. Roughness Characteristics of Prepared Hierarchically Structured Coatings by AFM

params	glass slide	$(70)(20)_4$	$(20)_3(70)(20)$	$(200)(20)_2$	$(200)(20)$	(200)
rms[a]	2.553	23.001	14.292	99.536	83.050	73.004
Ra[b]	2.089	17.587	11.285	90.568	69.948	60.524

[a]Root mean square average of height deviations taken from the mean image data plane. [b]Arithmetic average of the absolute values of the surface height deviations measured from the mean plane.

when large particles of 70 nm were used. Minor raspberry-like nanostructures appeared when large particles of 100 and 150 nm were used. Fine raspberry-like nanostructures formed only in the case of 200 nm large silica particles. It means that when the size ratio (r/R, r is the diameter of small silica particles and R is the diameter of large silica particles) is smaller than 1/10, fine raspberry-like nanostructures could be constructed. We compared the corresponding morphologies of coatings with 5 nanoparticles size ratios. In order to completely understanding the relation of size ratio and morphology, we also list the results of groups of Lee and Collinson in the Scheme 2. The groups of Lee and Collinson also used NPs of different sizes (70 nm/500 nm, 80 nm/450 nm, and 29 nm/1200 nm) but a similar size ratio for construction of raspberry-like structures.[43,44] It can be observed that raspberry-like nanostructures become finer, when the size ratio becomes smaller. Although Collinson's group used functionalized PS microspheres rather than silica particles to prepare raspberry-like particles, the driving forces for self-assembly were both the electrostatic force, and the size ratio could be analogously analyzed. Hierarchical structures like raspberry and strawberry were considered to be examples of aggregate fruits with high coverage of "satellite" (in the case of a raspberry) or low density of the "satellite" dispersed around the "core" (in the case of a strawberry), respectively. The ratio of satellite size to core size for 80/450 is bigger than 29/1200. Thus, steric hindrance and repulsive charge effects may become significant, making it harder to get raspberry-like structure like the 29/1200 one.[43] Beacuse of the same reason, the film morphology departs from the raspberry-like structure for the particles size ratios of 20/150, 70/500, 20/100, and 20/70.[44] The results of the current work are in good agreement with the above results obtained by the groups of Collinson and Lee. Thus, the raspberry-like structured surfaces can be fabricated using silica NPs pairs of appropriate size ratios. These results may give some guidelines for in situ constructing hierarchical structures by LbL assembly.

On the base of these hierarchically structured films, we further designed the $(PDDA/S\text{-}70)_1(PDDA/S\text{-}20)_4$ coating with mulberry-like hierarchical surface as shown in Figure 1e, f. The aggregated silica NPs appear like mulberries. AFM taping mode topography and 3D surface images are shown in Figure 3. Lots of small silica NPs aggregated on the large silica nanospheres so that mulberry-like clusters were observed instead of the large silica nanospheres. Meanwhile, the rms roughness of the $(PDDA/S\text{-}70)_1(PDDA/S\text{-}20)_4$ and $(PDDA/S\text{-}20)_3(PDDA/S\text{-}70)_1$ $(PDDA/S\text{-}20)_1$ coatings are 23.0 and 14.3 nm, respectively (Table 1). The films are smooth enough for use as AR coatings without much scattering of visible light and rough enough to enhance the hydrophilicity. The optical and wetting properties of all these coatings are discussed below.

Scheme 2. Schematic Illustration of All Size Ratios for Construction of Raspberry-like Structures in the Groups of Lee, Collinson (black), and He (red)[a]

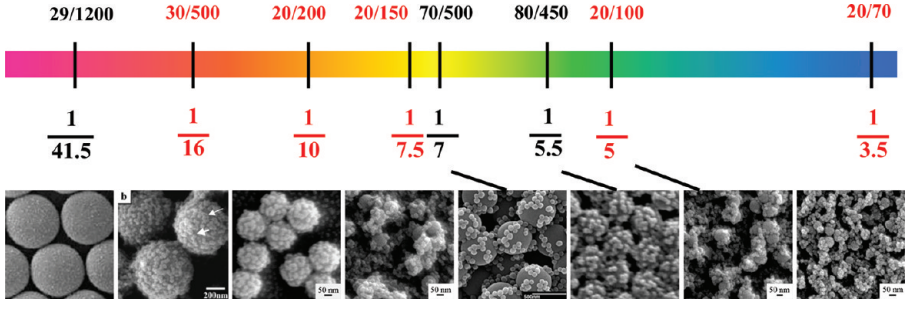

[a]The top line lists actual diameter (in nanometer) ratios. The second line lists the corresponding simple fractions of the size ratios. The bottom line shows the SEM images of corresponding particulate films.

dx.doi.org/10.1021/am3002082 | ACS Appl. Mater. Interfaces 2012, 4, 2204−2211

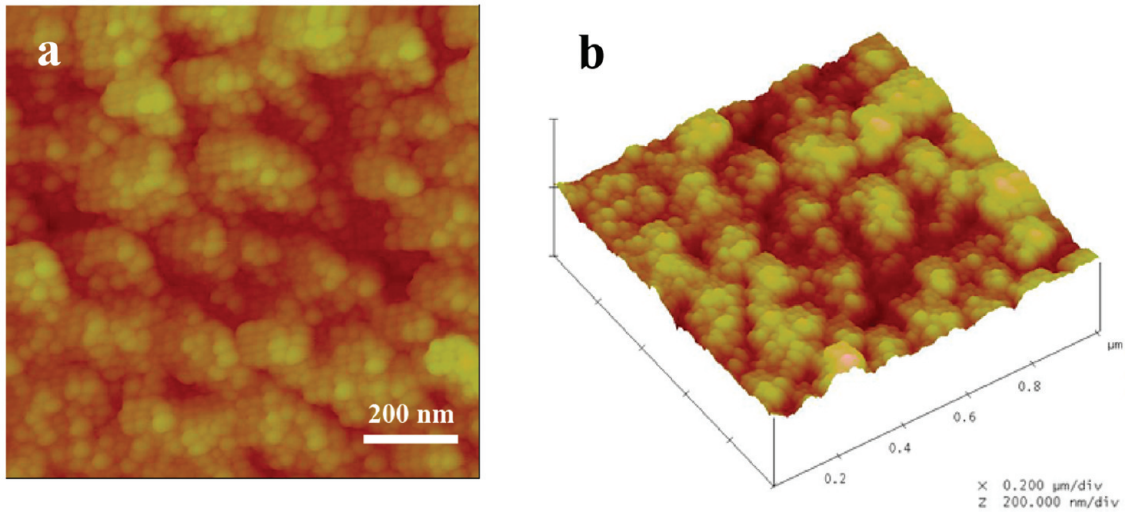

Figure 3. AFM tapping mode topography images of $(PDDA/S\text{-}70)_1(PDDA/S\text{-}20)_4$. (a) Top view and (b) side view.

Optical Properties of Coatings. The transmission spectra of control slide glass, slide glasses with $(PDDA/S\text{-}200)_1(PDDA/S\text{-}20)_2$, $(PDDA/S\text{-}200)_1(PDDA/S\text{-}20)_1$, and $(PDDA/S\text{-}200)_1$ coatings are shown in Figure 4. Large 200 nm particles layer decreases the transmittance of slide glass. The transmittance, however, increases with increase of the number of deposition cycles of (PDDA/S-20) bilayers, and clearly the (PDDA/S-20) bilayers enhanced the transmittance. The subsequently adsorbed NPs roughened the surface (rms showed in Tabel 1), and simultaneously formed new voids, which would reduce reflection and enhance transmission. As discussed above, the roughness and void fraction are supposed to increase with increasing the number of deposition cycles of NPs. Thus, void space with low refractive index (n = 1.0) is available for AR coatings. However, large voids would result in diffuse scattering. Therefore, optimal conditions need to be found to balance the void space and the concomitant diffuse scattering. Figure 5 shows the transmission spectra of control slide glass, slide glasses with $(PDDA/S\text{-}20)_3(PDDA/S\text{-}70)_1(PDDA/S\text{-}20)_1$, $(PDDA/S\text{-}20)_3(PDDA/S\text{-}100)_1(PDDA/S\text{-}20)_1$, and $(PDDA/S\text{-}20)_3(PDDA/S\text{-}150)_1$ $(PDDA/S\text{-}20)_1$ and $(PDDA/S\text{-}70)_1(PDDA/S\text{-}20)_4$ coatings. All these hierarchically structured coatings show the antireflective property. As discussed above, the large particles bilayer leading to large void and light-scatting will decrease the transmittance of

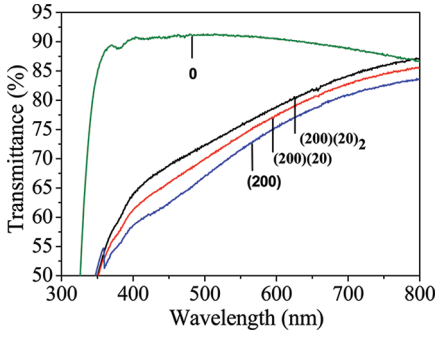

Figure 4. Transmission spectra of $(PDDA/S\text{-}200)_1(PDDA/S\text{-}20)_2$ (abbreviated as $(200)(20)_2$), $(PDDA/S\text{-}200)_1(PDDA/S\text{-}20)_1$ (abbreviated as (200)(20)) and $(PDDA/S\text{-}200)_1$ (abbreviated as (200)) after calcination. Line 0 is the spectrum of control slide glass.

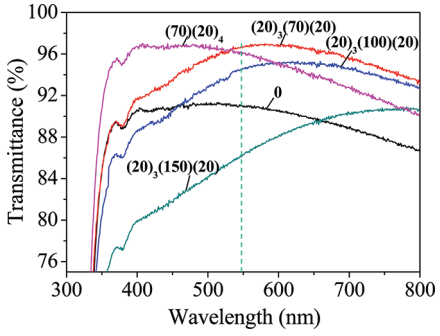

Figure 5. Transmission spectra of $(PDDA/S\text{-}70)_1(PDDA/S\text{-}20)_4$ (abbreviated as $(70)(20)_4$), $(PDDA/S\text{-}20)_3(PDDA/S\text{-}70)_1(PDDA/S\text{-}20)_1$ (abbreviated as $(20)_3(70)(20)$), $(PDDA/S\text{-}20)_3$ $(PDDA/S\text{-}100)_1(PDDA/S\text{-}20)_1$ (abbreviated as $(20)_3(100)(20)$), and $(PDDA/S\text{-}20)_3(PDDA/S\text{-}150)_1(PDDA/S\text{-}20)_1$ (abbreviated as $(20)_3(100)(20)$) after calcination. Line 0 shows the spectrum of control slide glass.

coatings. Nevertheless, the transmittance of $(PDDA/S\text{-}20)_3(PDDA/S\text{-}150)_1(PDDA/S\text{-}20)_1$ is still higher than that of the control slide glass between 650 and 800 nm. It means that NPs below 150 nm are available for fabricating particulate AR coatings. The maximum transmittances of $(PDDA/S\text{-}20)_3(PDDA/S\text{-}70)_1(PDDA/S\text{-}20)_1$ and $(PDDA/S\text{-}70)_1(PDDA/S\text{-}20)_4$ coatings were estimated to be 97.1 and 97.0%, respectively. The wavelength of maximum transmittance of $(PDDA/S\text{-}20)_3(PDDA/S\text{-}70)_1(PDDA/S\text{-}20)_1$ shifts to the red as compared with that of $(PDDA/S\text{-}70)_1(PDDA/S\text{-}20)_4$, which is probably attributed to different coating thickness and structure (e.g., surface roughness and void spaces, etc.), as revealed by comparison of Figure 1c and Figure S1a in the Supporting Information. Only five deposition cycles could achieve as high as 97% transmittance in both $(PDDA/S\text{-}20)_3(PDDA/S\text{-}70)_1(PDDA/S\text{-}20)_1$ and $(PDDA/S\text{-}70)_1(PDDA/S\text{-}20)_4$ coatings, as compared with 12 cycles needed in the previous work.[29] As we known, the LbL technique often needs lots of deposition cycles, which are time-consuming. Cutting down the number of deposition cycles can much save the assembly time and labor.

If a coating with the thickness (d_c) of $\lambda/4n_c$ (λ is the incidence wavelength) can reach zero reflection, the refractive

index of the coating should satisfy the criterion $n_c = (n_a n_s)^{1/2}$ (1), where n_c, n_a, and n_s are the refractive indices of the coating, air and substrate, respectively. Here, the value of n_a can be approximated as 1. For most glass and plastics, the value of n_s is ~1.5. Thus the value of n_c can be calculated to be 1.23.[45] That is the general and approximate theory described earlier. For the current porous nanoparticles coatings, we can regard the coating and glass substrate as a whole bulk film with a certain thickness of d_{bulk} and the refractive index of n_{bulk}. When λ is close to $4d_c n_c$, this coating can reach the minimum reflection and the eq 2 can be applied

$$n_{bulk} = n_c^2/n_s \quad (2)$$

and as already known,

$$R = (n_{bulk} - 1)^2/(n_{bulk} + 1)^2 \quad (3)$$

where R is the reflectance of bulk film.

So as to slide glass with the AR coating, it satisfys the criterions below

$$R_s = (n_s - 1)^2/(n_s + 1)^2 \quad (4)$$

$$R = (n_c^2/n_s - 1)^2/(n_c^2/n_s + 1)^2 \quad (5)$$

The slide glass with $(PDDA/S\text{-}20)_3(PDDA/S\text{-}70)_1(PDDA/S\text{-}20)_1$ coating has the minimum reflection (R_{min}) when λ is 560 nm. It is noted that R in the equation is the single surface reflectance. The minimum reflectance can be calculated from the maximum transmittance if the absorption is neglected, i.e., $R_{min} = 1 - T_{max}$. For example, the R_{min} of the slide glass with $(PDDA/S\text{-}20)_3(PDDA/S\text{-}70)_1(PDDA/S\text{-}20)_1$ coating (T_{max} = 97%) was estimated to be 3.0%. The reflection calculated is attributed to the both surfaces of slide glass with AR coatings. According to eq 3, $R_{single} = R_{min}/2 = (n_{bulk} - 1)^2/(n_{bulk} + 1)^2$ = 1.5%, the n_{bulk} was calculated to be 1.29. The tranmittance of glass substrate is 90.7% at the wavelength of 560 nm, and the single surface reflectance of glass substrate (R_s) at this wavelength was similarly calculated to be 9.3%/2 = 4.6% (Figure 5). n_s was thus calculated to be 1.54 from the equation $R_s = (n_s - 1)^2/(n_s + 1)^2$. Therefore, n_c was calculated to be 1.41 at the wavelength of 560 nm according to eq 2. The n_c values of other coatings were also calculated and listed in Table 2. The

Table 2. Parameters of AR Coatings at the Wavelength of the Minimum Reflection

params	$(70)(20)_4$	$(20)_3(70)(20)$	$(20)_3(100)_1(20)_1$	$(20)_3(150)_1(20)_1$
d	85.5	99.3	101.9	106.9
n_c	1.40	1.41	1.46	1.59
λ (nm)	479	560	595	680
R_{min} (5)	1.6	1.6	2.4	4.6

reflective index increases by using larger NPs, resulting in the increase of reflection. The thickness and reflective index of slide glass with $(PDDA/S\text{-}20)_3(PDDA/S\text{-}70)_1(PDDA/S\text{-}20)_1$ coating were also measured by spectroscopic ellipsometry, and they are 122.8 nm and 1.206, respectively. A general trend of the refractive index and the thickness of coatings could be seen in Table 2. Clearly, the current LbL method could regulate the n_c at the wavelength of minimum reflection by choosing silica nanoparticles of varied sizes. Moreover, the wavelength of the minimum reflection could be controlled by varying the deposition sequence of identical combination of different nanoparticles .

Wetting Property and Antifogging Function of Coatings. According to early theoretical works by Wenzel[47] and Quéré et al,[48,49] void fraction and surface roughness would significantly affect the wettability of a surface with water. When a surface has a WCA of <5° after a spreading time of 0.5 s or less, it is defined as superhydrophilic. Previous studies by our goup[20,21,30] and by Rubner and co-workers[26,50] pointed out that the high level of wettabilty of silica NPs coupled with the rough and nanoporous nature of multilayer coatings establish ideal conditions for extreme superhydrophilic behaviors. As for antifogging coatings, the spreading time of water droplets is a very important factor to be considered. Figure 6 shows time-dependent changes in WCA on $(PDDA/S\text{-}200)_1(PDDA/S\text{-}20)_2$, $(PDDA/S\text{-}200)_1(PDDA/S\text{-}20)_1$ and $(PDDA/S\text{-}200)_1$ coatings. The volume of water droplets for the measurements was 3 μL. The water droplet spreading of $(PDDA/S\text{-}200)_1$ coating is the slowest because it does not have the second-level structure, and thus has the smallest roughness (73.0 nm). The WCA on the roughest surface of $(PDDA/S\text{-}200)_1(PDDA/S\text{-}20)_2$ coating (99.5 nm) is lower than on the surface of $(PDDA/S\text{-}200)_1$ coating but larger than on $(PDDA/S\text{-}200)_1(PDDA/S\text{-}20)_1$ coating (83.1 nm). Water droplets spread faster on the $(PDDA/S\text{-}200)_1(PDDA/S\text{-}20)_2$ coating than on the $(PDDA/S\text{-}200)_1$ coating, but slower than on the $(PDDA/S\text{-}200)_1(PDDA/S\text{-}20)_1$ coating. That means the surface roughness is not the only determinant in the wettability of a surface with water. Our previous results also indicated that not the roughest coating has the fastest spreading speed.[29] The effective void fraction also enhances the spreading flat of water droplets. Time-dependent changes in WAC are shown in Figure 7 as a function of $(PDDA/S\text{-}20)_3(PDDA/S\text{-}70)_1(PDDA/S\text{-}20)_1$ and $(PDDA/S\text{-}70)_1(PDDA/S\text{-}20)_4$ coatings. Clearly, the surface wettability of $(PDDA/S\text{-}70)_1(PDDA/S\text{-}20)_4$ coating is better than that of $(PDDA/S\text{-}20)_3(PDDA/S\text{-}70)_1(PDDA/S\text{-}20)_1$ coating due to the increase of surface roughness (Table 1). The spreading time on the $(PDDA/S\text{-}70)_1(PDDA/S\text{-}20)_4$ coating is as short as 0.39 s when water droplets of 3 μL are used. This mulberry-like surface exhibits good surperhydrophilic which doubtlessly meets the requirements of antifogging coatings. Therefore, the antifogging behavior of the superhydrophilic mulberry-like hierarchical structure coating was studied. A control slide glass and a slide glass with (PDDA/S-

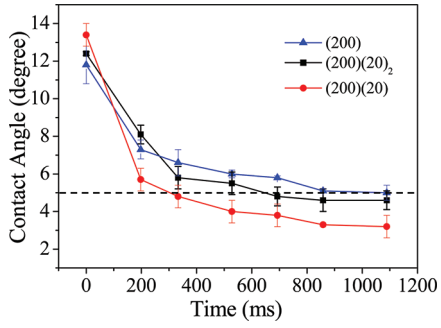

Figure 6. Time-dependent changes in instant contact angle as a function of $(PDDA/S\text{-}200)_1(PDDA/S\text{-}20)_2$ (abbreviated as (200)$(20)_2$), $(PDDA/S\text{-}200)_1(PDDA/S\text{-}20)_1$ (abbreviated as (200)(20)), and $(PDDA/S\text{-}200)_1$ (abbreviated as (200)). Water droplets of 3 μL were applied in all the measurements.

dx.doi.org/10.1021/am3002082 | ACS Appl. Mater. Interfaces 2012, 4, 2204−2211

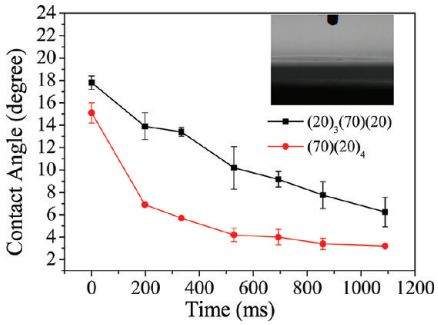

Figure 7. Time-dependent changes in instant contact angle as a function of $(PDDA/S\text{-}70)_1(PDDA/S\text{-}20)_4$ (abbreviated as $(70)(20)_4$), $(PDDA/S\text{-}20)_3(PDDA/S\text{-}70)_1(PDDA/S\text{-}20)_1$ (abbreviated as $(20)_3(70)(20)$). Inset is a static contact angle image of $(70)(20)_4$.

$70)_1(PDDA/S\text{-}20)_4$ coating were cooled at ca. −15 °C for 3 h in a refrigerator, and then exposed to humid laboratory air (ca.20% RH). As shown in the upper parts of Figure 8a and b,

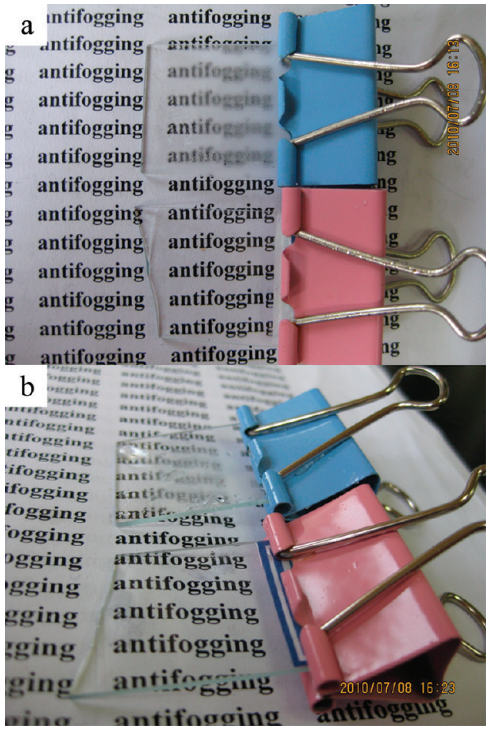

Figure 8. (a) Top view and (b) side view digital images exhibiting antifogging property of slide glass deposited on both sides with $(PDDA/S\text{-}70)_1(PDDA/S\text{-}20)_4$ (abbreviated as $(70)(20)_4$)) (lower) in combination with control slide glass (upper). Both slides were cooled at ca. −15 °C for 3 h in a refrigerator, and then exposed to humid laboratory air (ca. 20% RH).

the control slide glass fogged immediately. In contrast, the slide glass with $(PDDA/S\text{-}70)_1(PDDA/S\text{-}20)_4$ coating remained clear (lower parts in both pictures). Unlike the previous works in which relatively large raspberry-like NPs were used as building block[28,30] and the coatings became clear (>90%) only when the sheet-like wetting by water prevented light scatting, the current coating exhibits high transparency under both dry and wet conditions. That may be because the previous raspberry-like particulate coatings with large particles (>150 nm) are so rough as to show low transparency due to diffuse scatting under dry conditions, whereas the appropriate void fraction and surface roughness of mulberry-like coating is in favor of the antireflective behavior both under dry and under wet conditions.

4. CONCLUSIONS

Raspberry-like and mulberry-like hierarchically structured silica coatings were prepared via a facile in situ approach with particles of two sizes. These hierarchically structured coatings with large surface roughness and nanovoids showed exciting superhydrophilic and antifogging properties. When the size ratio of two particles was less than 1/10, raspberry-like nanostructures were obtained. When particles of closer sizes (20 nm/70 nm) were used, however, mulberry-like hierachically structured AR coatings $((PDDA/S\text{-}70)_1(PDDA/S\text{-}20)_4)$ were fabricated by only five LbL deposition cycles of PDDA/silica NPs bilayers. The number of adsorption cycles was significantly cut down, as compared with 12 deposition cycles needed in our previous work for reaching a similar high transmittance of 97.0%. This fabrication process would much reduce the labor and time needed, overcoming the time-consuming disadvantage which interferes the application of the LbL technique. Therefore, the current work would provide a simple, versatile way and a blue print for designing the combination of nanopartiles of varied sizes to fabricate hierarchical nanostructures for AR and antifogging coatings.

■ ASSOCIATED CONTENT

Supporting Information

SEM images of $(PDDA/S\text{-}20)_3(PDDA/S\text{-}70)_1(PDDA/S\text{-}20)_1$, $(PDDA/S\text{-}20)_3(PDDA/S\text{-}100)_1(PDDA/S\text{-}20)_1$, and $(PDDA/S\text{-}20)_3(PDDA/S\text{-}150)_1(PDDA/S\text{-}20)_1$ coatings are observed. This material is available free of charge via the Internet at http://pubs.acs.org/.

■ AUTHOR INFORMATION

Corresponding Author

*Tel/Fax: +86 10 82543535. E-mail: jhhe@mail.ipc.ac.cn.

Notes

The authors declare no competing financial interest.

■ ACKNOWLEDGMENTS

This work was supported by the Knowledge Innovation Program of the Chinese Academy of Sciences (CAS) (Grants KGCX2-YW-370, KGCX2-EW-304-2), the National High Technology Research and Development Program ("863" Program) of China (Grant 2011AA050525), and "Hundred Talents Program" of CAS. We thank Semilab Semiconductor Physics Laboratory Co. Ltd. for measuring the reflective index and thickness of slide glass with $(PDDA/S\text{-}20)_3(PDDA/S\text{-}70)_1(PDDA/S\text{-}20)_1$ coating using their spectroscopic ellipsometer.

■ REFERENCES

(1) Matsushita, S. I.; Miwa, T.; Tryk, D. A.; Fujishima, A. *Langmuir* **1998**, *14*, 6441.
(2) Walheim, S.; Schffer, E.; Mlynek, J.; Steiner, U. *Science* **1999**, *283*, 520.
(3) Sharma, A. C.; Borovik, A. S. *J. Am. Chem. Soc.* **2000**, *122*, 8946.
(4) Zhao, Y.; Zhang, X.; Zhai, J.; He, J.; Jiang, L.; Liu, Z.; Nishimoto, S.; Murakami, T.; Fujishima, A.; Zhu, D. *Appl. Catal. B: Environ.* **2008**, *83*, 24.
(5) Liu, H.; Feng, L.; Zhai, J.; Jiang, L.; Zhu, D. *Langmuir* **2004**, *20*, 5659.

(6) Kidoaki, S.; Kwon, I. K.; Matsuda, T. *Biomaterials* **2005**, *26*, 37.
(7) Li, Y. Y.; Cunin, F.; Link, J. R.; Gao, T.; Betts, R. E.; Reiver, S. H.; Chin, V.; Bhatia, S. N.; Sailor, M. J. *Science* **2003**, *299*, 2045.
(8) Li, M.; Zhai, J.; Liu, H.; Song, Y.; Jiang, L.; Zhu, D. *J. Phys. Chem. B* **2003**, *107*, 9954.
(9) Li, Y.; Li, C.; Cho, S. O.; Duan, G.; Cai, W. *Langmuir* **2007**, *23*, 9802.
(10) Jiang, L.; Zhao, Y.; Zhai, J. *Angew. Chem., Int. Ed.* **2004**, *116*, 4438.
(11) Xiu, Y.; Zhu, L.; Hess, D. W.; Wong, C. *Nano Lett.* **2007**, *7*, 3388.
(12) Qian, B.; Shen, Z. *Langmuir* **2005**, *21*, 9007.
(13) Zhu, Y.; Zhang, J.; Zheng, Y.; Huang, Z.; Feng, L.; Jiang, L. *Adv. Funct. Mater.* **2006**, *16*, 568.
(14) Feng, X.; Zhai, J.; Jiang, L. *Angew. Chem., Int. Ed.* **2005**, *44*, 5115.
(15) Li, Y.; Cai, W.; Duan, G.; Cao, B.; Sun, F.; Lu, F. *J. Colloid Interface Sci.* **2005**, *287*, 634.
(16) Liu, K.; Zhai, J.; Jiang, L. *Nanotechnology* **2008**, *19*, 165604.
(17) Tsai, P. S.; Yang, Y. M.; Lee, Y. L. *Nanotechnology* **2007**, *18*, 465604.
(18) Feng, X. J.; Jiang, L. *Adv. Mater.* **2006**, *18*, 3063.
(19) Feng, L.; Li, S.; Li, Y.; Li, H.; Zhang, L.; Zhai, J.; Song, Y.; Liu, B.; Jiang, L.; Zhu, D. *Adv. Mater.* **2002**, *14*, 1857.
(20) Du, X.; Li, X. Y.; He, J. H. *ACS Appl. Mater. Interface* **2010**, *2*, 2365.
(21) Li, X.; Du, X.; He, J. *Langmuir* **2010**, *26*, 13528.
(22) Song, S.; Jing, L.; Li, S.; Fu, H.; Luan, Y. *Mater. Lett.* **2008**, *62*, 3503.
(23) Zhang, L.; Chen, H.; Sun, J.; Shen, J. *Chem. Mater.* **2007**, *19*, 948.
(24) Li, Y.; Sasaki, T.; Shimizu, Y.; Koshizaki, N. *J. Am. Chem. Soc.* **2008**, *130*, 14755.
(25) Zhai, L.; Berg, M. C.; Cebeci, F. C.; Kim, Y.; Milwid, J. M.; Rubner, M. F.; Cohen, R. E. *Nano Lett.* **2006**, *6*, 1213.
(26) Lee, D.; Rubner, M. F.; Cohen, R. E. *Nano Lett.* **2006**, *6*, 2305.
(27) Zhang, X. T.; Sato, O.; Taguchi, M.; Einaga, Y.; Murakami, T.; Fujishima, A. *Chem. Mater.* **2005**, *17*, 696.
(28) Liu, X.; Du, X.; He, J. *Chemphyschem* **2008**, *9*, 305.
(29) Liu, X.; He, J. *J. Phys. Chem. C* **2009**, *113*, 148.
(30) Liu, X.; He, J. *J. Colloid Interface Sci.* **2007**, *314*, 341.
(31) Du, X.; Liu, X.; Chen, H.; He, J. *J. Phys. Chem. C* **2009**, *113*, 9063.
(32) Wang, M. F.; Raghunathan, N.; Ziaie, B. *Langmuir* **2007**, *23*, 2300.
(33) Shi, F.; Wang, Z.; Zhang, X. *Adv. Mater.* **2005**, *17*, 1005.
(34) Zhao, N.; Xie, Q.; Weng, L.; Wang, S.; Zhang, X.; Xu, J. *Macromolecules* **2005**, *38*, 8996.
(35) Hayakawa, T.; Horiuchi, S. *Angew. Chem., Int. Ed.* **2003**, *42*, 2285.
(36) Wang, M.; Comrie, J. E.; Bai, Y.; He, X.; Guo, S.; Huck, W. T. S. *Adv. Funct. Mater.* **2009**, *19*, 2236.
(37) Cao, L.; Price, T. P.; Weiss, M.; Gao, D. *Langmuir* **2008**, *24*, 1640.
(38) Shi, F.; Chen, X.; Wang, L.; Niu, J.; Yu, J.; Wang, Z.; Zhang, X. *Chem. Mater.* **2005**, *17*, 6177.
(39) Liu, X.; He, J. *Langmuir* **2009**, *25*, 11822.
(40) D'Acunzi, M.; Mammen, L.; Singh, M.; Deng, X.; Roth, M.; Auernhammer, G. K.; Butt, H.-J.; Vollmer, D. *Faraday Discuss.* **2010**, *146*, 35.
(41) Luckham, P.; Vincent, B.; Hart, C.; Tadros, T. F. *Colloids Surf.* **1980**, *1*, 281.
(42) Wagner, C. S.; Shehata, S.; Henzler, K.; Yuan, J.; Wittemann, A. *J. Colloid Interface Sci.* **2011**, *355*, 115.
(43) Zhao, B.; Collinson, M. M. *Chem. Mater.* **2010**, *22*, 4312.
(44) Tsai, H.-J.; Lee, Y.-L. *Langmuir* **2007**, *23*, 12687.
(45) Bravo, J.; Zhai, L.; Wu, Z.; Cohen, R.; Rubner, M. *Langmuir* **2007**, *23* (13), 7293−7298.
(46) StÖber, W.; Fink, A.; Bohn, E. *J. Colloid Interface Sci.* **1968**, *26*, 62.
(47) Wenzel, R. *Ind. Eng. Chem.* **1936**, *28*, 988.
(48) Bico, J.; Marzolin, C.; Quéré, D. *Europhys. Lett.* **1999**, *47*, 220.
(49) Bico, J.; Tordeux, C.; Quéré, D. *Europhys. Lett.* **2001**, *55*, 214.
(50) Cebeci, F. C.; Wu, Z.; Zhai, L.; Cohen, R. E.; Rubner, M. F. *Langmuir* **2006**, *22*, 2856.